

Boise State University ScholarWorks

Physics Faculty Publications and Presentations

Department of Physics

9-16-2009

The Influences of Cell Type and ZnO Nanoparticle Size on Immune Cell Cytotoxicity and Cytokine Induction

Cory Hanley

Boise State University

Aaron Thurber

Boise State University

Charles Hanna

Boise State University

Alex Punnoose

Boise State University

Jianhui Zhang

Boise State University

See next page for additional authors

This is an author-produced, peer-reviewed version of this article. The final, definitive version of this document can be found online at *Nanoscale Research Letters*, published by Springer. Copyright restrictions may apply. DOI: [10.1007/s11671-009-9413-8](https://doi.org/10.1007/s11671-009-9413-8)

Authors

Cory Hanley, Aaron Thurber, Charles Hanna, Alex Punnoose, Jianhui Zhang, and Denise G. Wingett

The Influences of Cell Type and ZnO Nanoparticle Size on Immune Cell Cytotoxicity and Cytokine Induction

Cory Hanley¹, Aaron Thurber², Charles Hanna², Alex Punnoose²,
Jianhui Zhang², and Denise G. Wingett^{1,3,4}

¹Department of Biological Sciences, Boise State University, Boise, ID 83725

²Department of Physics, Boise State University, Boise, ID 83725

³Department of Medicine, Division of Gerontology and Geriatric Medicine,
University of Washington, Seattle, WA 98195

⁴MSTMRI Research Institute of St. Luke's Regional Medical Center, Boise, ID, 83712

Corresponding Author: Dr. Denise Wingett, Department of Biological Sciences, Boise State University,
1910 University Dr., Boise, ID 83725. Fax: (208) 426-1040, Tel: (208) 426-2921. E-mail address:
denisewingett@boisestate.edu

Keywords: nanoparticle, ZnO, T lymphocyte, monocytes, cytokine, immunity, nanotoxicity

Abstract

Nanotechnology represents a new and enabling platform that promises to provide a range of innovative technologies for biological applications. ZnO nanoparticles of controlled size were synthesized, and their cytotoxicity towards different human immune cells evaluated. A differential cytotoxic response between human immune cell subsets was observed, with lymphocytes being the most resistant and monocytes being the most susceptible to ZnO nanoparticle-induced toxicity. Significant differences were also observed between previously activated memory lymphocytes and naive lymphocytes, indicating a relationship between cell-cycle potential and nanoparticle susceptibility. Mechanisms of toxicity involve the generation of reactive oxygen species, with monocytes displaying the highest levels, and the degree of cytotoxicity dependent on the extent of nanoparticle interactions with cellular membranes. An inverse relationship between nanoparticle size and cytotoxicity, as well as nanoparticle size and reactive oxygen species production was observed. In addition, ZnO nanoparticles induce the production of the proinflammatory cytokines, IFN- γ , TNF- α and IL-12, at concentrations below those causing appreciable cell death. Collectively, these results underscore the need for careful evaluation of ZnO nanoparticle effects across a spectrum of relevant cell types when considering their use for potential new nanotechnology-based biological applications.

Introduction

Nanotechnology permits the manipulation of matter at the nanometer scale which enables precision engineering to control nanomaterial physiochemical properties as well as their interactions with biological systems. It is the alterations in electrical, magnetic, structural, morphological, chemical, and physical properties of nanomaterials, which are comparable in size to naturally occurring biomolecules, that makes them particularly attractive for pioneering applications in technological and biological applications [1-4]. Nanomaterials comprised of ZnO have received considerable attention in recent years because of their potential use in electronic and industrial applications arising from their wide band-gap (3.36 eV) semiconductor properties [3]. From a biological perspective, nanoscale ZnO materials are already being used in the cosmetic and sunscreen industry due to their transparency and ability to reflect, scatter, and absorb UV radiation, and as food additives [5,6]. ZnO nanomaterials are also being considered for use in next-generation biological applications including antimicrobial agents, drug-delivery, bioimaging probes and cancer treatment [7-10]. Although bulk (micron-sized) ZnO is generally recognized as a GRAS substance by the FDA [5,6], many benign materials can exhibit appreciable cellular toxicity when reduced to the nanoscale [11]. Recent toxicological studies using certain engineered nanoparticles (NPs) have confirmed the potentially harmful effects due to their high surface area, unique physiochemical properties, and increased reactivity of the material's surface [11,12]. This has led to the term, *nanotoxicology*, which describes the relationship between nanoparticle physiochemical properties, and toxicological effects on living cells and biological systems.

In this regard, several recent reports have demonstrated the toxicity of metal-oxide NPs to both prokaryotic and eukaryotic cellular systems [7,7,10,13-16], while the bulk micron-sized materials remain non-toxic. The majority of eukaryotic studies specific to ZnO NPs, however, have relied heavily on the use of immortalized cells lines, which are recognized to display altered sensitivities to foreign materials/chemicals due to alterations in metabolic processes and major genetic instabilities. To date, only limited studies have evaluated the toxicity of ZnO NPs on normal primary human cells and their potential immunomodulatory effects. Even more challenging is the fact that the cytotoxic response is very different between cell types and nanomaterial systems, making it difficult to develop predictive models without detailed and systematic investigations. Recent reports demonstrate that ZnO NPs display differential toxicity towards primary human cells depending upon their proliferation potential, with normal T lymphocytes that are stimulated to divide by signaling through the T cell receptor displaying significantly greater toxicity than quiescent nonproliferating cells of identical lineage [13]. When these studies were extended to immortalized T leukemic and lymphoma cells using identical ZnO NPs, an even greater sensitivity to NP-induced toxicity was observed (~33-fold) [13]. Thus, susceptibility to NP-induced cytotoxicity appears to be related to the proliferative capacity of the cell, and may also be affected by other physiologically relevant parameters, including cell-NP electrostatic interactions and inherent differences in cellular endocytic/phagocytic processes that facilitate NP uptake. These variations in cytotoxic response indicate that a more detailed and carefully controlled evaluation of ZnO NP effects on multiple types of normal human cells is needed to better understand the biological consequences of NP exposure. In addition, it is increasingly being recognized that toxicity depends on nanomaterial characteristics including size, shape, and electrostatic charge, as well as materials composition [7,10,17,18]. In this study, the evaluation of size-controlled ZnO NPs and their resulting toxicity on different cells comprising the human immune system is explored. In addition, mechanisms underlying the differential toxicity response are investigated, as well as effects of ZnO NPs to induce pro-inflammatory cytokine expression.

Experimental

Preparation and Characterization of ZnO Nanoparticles

ZnO NPs utilized in all experiments were synthesized in diethylene glycol (DEG) via forced hydrolysis of zinc acetate [14]. In brief, zinc acetate was dissolved in DEG, and then nanopure water was added under magnetic stirring. Subsequently, the system was heated at 160 °C under reflux for 90 min. After cooling, the resulting product was removed from DEG via centrifugation, and washed with ethanol several times before drying for 24 hours at 50°C, resulting in a powder sample. The sample crystal phase, crystallite size,

and morphology were characterized via x-ray diffraction (XRD) and transmission electron microscopy (TEM) as previously described [13,14]. The NPs were then weighed and reconstituted in phosphate buffered saline (PBS) solution to the desired stock concentration. After reconstitution, NPs were sonicated for 10 minutes and immediately vortexed prior to addition to cell cultures.

Isolation of Peripheral Blood Mononuclear Cells

For isolation of PBMC (peripheral blood mononuclear cells) and immune cell subsets, written informed consent was obtained from all blood donors. The University Institutional Review Board approved this study. PBMC were obtained via Ficoll-Hypaque (Histopaque-1077, Sigma, St Louis, MO) gradient centrifugation using heparinized phlebotomy samples [19]. After removal of the leukocyte layer, cells were washed three times with Hank's buffer (Sigma, St. Louis, MO) and resuspended at a final concentration of 1×10^6 cells/ml in RPMI-1640 (Sigma) containing 10% fetal bovine serum (FBS) and cultured at 37° C and 5% CO₂.

Isolation and Culture of Primary CD14⁺ Monocytes and CD4⁺ T cells

PBMC were obtained by Ficoll-Hypaque density centrifugation as described above, and CD14⁺ cells isolated from the mixed cell suspension. Negative immunomagnetic selection was performed according to the manufacturer's protocol using a cocktail of antibodies directed against CD2, CD3, CD16, CD19, CD20, CD56, CD66b, CD123, and glycophorin A (StemCell Technologies, Vancouver, BC). For optimal cell recovery, PBMC were first blocked with anti-human CD32 (Fcγ RII) blocker reagent before labeling with the antibody cocktail. Purified CD14⁺ monocytes populations were typically of >92% purity and >97% viable as assessed by flow cytometry and cultured in RPMI/10% FBS at 5×10^5 cells/ml in 96-well plates at 37° C and 5% CO₂.

CD4⁺ T cells were purified from PBMC using negative immunomagnetic selection per manufacturer's instructions and a cocktail of antibodies directed against CD8, CD14, CD16, CD19, CD56, and glycophorin A surface markers (StemCell Technologies). Unlabeled T cells were collected (typically >97% purity and > 95% viable as assessed by flow cytometry) and subsequently cultured in RPMI/10% FBS at a final concentration of 1×10^6 cells/ml.

Flow Cytometry

Methods of immunofluorescent staining and flow cytometric analysis were performed as previously described [19] using a 4-color Epics XL flow cytometer (Beckman Coulter, Miami, FL). Cells were stained with fluorescently labeled antibodies (Beckman Coulter) for 30 min at 4°C, washed two times, and immediately analyzed. Ten thousand events gated on the parameter of size (forward scatter, or FS) and granularity (side scatter, or SSC) were analyzed, and expression of the percentage of positively staining cells and the mean fluorescence intensity (MFI) determined by comparisons to isotype controls. Appropriate concentrations of each antibody were determined by titration for optimal staining prior to experimental use. In PBMC cultures, individual cell types were distinguished from one another based on differential antibody staining and on FS and SSC properties. T cells were defined as CD3⁺; T helper cells defined as CD3⁺,CD4⁺; naïve T cells defined as CD3⁺,CD45RA⁺; memory T cells defined as CD3⁺,CD45RO⁺; B cells defined as CD19⁺,CD3⁺; NK cells defined as CD56⁺,CD16⁺,CD3⁺, and monocytes defined as CD14⁺,CD3⁺. To prevent indiscriminate antibody staining of monocytes via Fc receptors, 100 µl of heat-inactivated human AB serum was added to experimental samples immediately prior to staining.

Cell Viability Assays

Cell viability following NP treatment was assessed using two different assays. In the first assay, cell subsets were identified using fluorescently labeled antibodies, and viability was determined by staining with 50 µg/ml of propidium iodide (PI) to monitor losses in cell membrane integrity. Fluorescent CountBright counting beads (Invitrogen, Carlsbad, CA) were added to samples to enable determinations of absolute cell numbers, and flow cytometry was used to evaluate changes in PI staining and to quantify cell death. NPs were excluded from the analysis based on absence of fluorescence signal and light FS and SSC characteristics.

The second viability assay employed the fluorogenic redox indicator dye, Alamar Blue. This dye becomes fluorescent upon reduction by mitochondrial enzymes in metabolically active cells. Cell populations were seeded into 96-well plates at 5×10^5 cells/ml, treated with ZnO NP for 18h, and 20 μ l of Alamar Blue added to cultures for an additional 6h. Changes in fluorescence were evaluated spectrophotometrically using excitation/emission at 530/590 nm.

ROS Detection

To assay for NP-induced reactive oxygen species (ROS) production, cells were first obtained from whole blood treated with an ammonium chloride lysing solution (1.5 M NH_4Cl , 0.1 M NaHCO_3 , 0.01 EDTA) to lyse red blood cells, and centrifuged for 10 min at 4°C to remove erythrocytic debris. The white blood cells were then resuspended in phenol red-free RPMI to a final concentration of 1×10^6 cells/ml, and incubated with ZnO NPs for 6h to 20h. Cells were subsequently loaded with 5 μM of the oxidation-sensitive dye, 2',7'-dichlorofluorescein diacetate (DCFH-DA, Invitrogen, Carlsbad, CA) for 20 min. Production of the oxidation product was evaluated using flow cytometry as previously described [20]. White blood cell populations (i.e., $\text{CD}3^+$ T cells and $\text{CD}14^+\text{CD}3^-$ monocytes) present in the samples were simultaneously evaluated based on FS and SSC gating and staining with appropriate fluorescently labeled antibodies. As a positive control for ROS production, control cells were loaded with DCFH-DA dye and activated with PMA (25 ng/mL) for 1h. For studies described in Figure 7, ROS production was evaluated in PBMC treated with different-sized ZnO NPs using a fluorescent microplate reader as previously described [21,22]. Experimental methodology, including the use of the DCFH-DA dye to indicate ROS generation, was identical as described above.

To determine the role of ROS in NP-induced cell death, purified primary $\text{CD}4^+$ T cells and monocytes were seeded in a 96-well plate at 5×10^5 cells/ml and pre-treated with 5 mM of the ROS scavenger, N-acetyl cysteine (NAC, Sigma), for 4-6h. Cultures were then treated with various concentrations of ZnO NP for 24h and viability was determined using the Alamar Blue cytotoxicity assay and a fluorescent microplate reader.

Cytokine Analysis

To investigate the effect of ZnO NPs on cytokine production, an ELISA (enzyme linked immunosorbent assay) was used. For determination of $\text{IFN-}\gamma$ and $\text{TNF-}\alpha$ production, freshly isolated PBMC were cultured at 1×10^6 cells/mL, and treated with varying concentrations of 8-nm ZnO NPs (0.05 mM, 0.1 mM and 0.2 mM) for 38h. For determination of IL-12 levels, PBMC cultures were either left untreated or pretreated with 1000 U/mL of $\text{IFN-}\gamma$ (Peprotech, Rocky Hill, NJ), to prime for the production of this cytokine, and then cultured with ZnO NPs for 24h. After NP treatment, cell-free supernatants were harvested via successive 10-min centrifugations (2,000 rpm, 7,000 rpm and 13,000 rpm) and stored at -80°C until analysis. ELISA was performed by the UMAB Cytokine Core Laboratory (Baltimore, MD), with all samples analyzed in triplicate.

Statistical Analyses

All data was analyzed using SAS, Inc. software (Cary, NC). Data for figures 3, 4, and 6 was analyzed using repeated measures of variance with *post hoc* comparisons to allow within-subject variation to be separated from between-subject variation. Data for figures 5, 7 and 8 was analyzed using a two-way analysis of variance (ANOVA). In all cases, significance levels were defined as $p < 0.05$.

Results and Discussion

Synthesis and Size Control of ZnO Nanoparticles

To evaluate the relationship between NP size and cytotoxic properties on various types of immune cells, ZnO NPs (4-20 nm) were synthesized by modifying the hydrolysis molar ratio of water to zinc acetate. Transmission electron microscopy (TEM) measurements shown in Figure 1a-d demonstrate that the use of hydrolysis ratios (water:zinc acetate) of 2.4, 6.1, 12.2, and 24.4 yields NPs with average diameters of 4 to 8, 13, and 20 nm, respectively. The 4 nm NP produced by this synthesis method are of roughly spherical in morphology while $\text{NPs} \geq 8$ nm acquire a rod-shaped morphology. The corresponding particle-size

histogram (Figure 1e) shows that all of the ZnO samples have a narrow size distribution. The x-ray diffraction (XRD) patterns shown in Figure 2 indicate that all of the ZnO samples are well-indexed to the pure wurtzite crystallite phase of ZnO, demonstrating that the sample is comprised of ZnO nanocrystals. Furthermore, the average crystallite sizes estimated using the peak widths (full width at half maximum) of the XRD patterns agree well with TEM results for both size and shape, where the average aspect ratio of NPs > 8nm increases up to 2 (Figure 2 inset).

T and B Lymphocytes are More Resistant to NP Toxicity Compared to Monocytes and NK Cells

Previous studies from our laboratory have determined that rapidly dividing cancerous T cells are more susceptible to ZnO NP toxicity than normal quiescent T cells [13]. These findings were extended to determine whether NP toxicity might also vary between different types of normal cells comprising the human immune system including T cells, B cells, natural killer (NK) cells, and monocytes. For these studies, freshly isolated peripheral blood mononuclear cell (PBMC) preparations were used, since all of the desired cell types for study are present in the same culture allowing for a well-controlled and uniform NP exposure. Following 24h NP treatment, the various cell types were identified by staining with antibodies specific for T, B, NK or monocyte surface markers, and NP-induced cytotoxicity was assessed using propidium iodide (PI), which is a red fluorescent nuclear stain that selectively enters cells with disrupted plasma membranes. As shown in Figure 3A, differences in NP-induced cytotoxicity were apparent with lymphocytes (CD3⁺ T cells, CD4⁺ T cells, and B cells) displaying the most resistance. All of these lymphocyte populations displayed similar IC₅₀ values (~ 5.0 mM), with no significant difference observed between them at any NP concentration evaluated. In contrast, NK cells were substantially more sensitive to NP-induced cytotoxicity, with an IC₅₀ of ~1.0 mM. Statistically significant differences were detected between NK cells and B and T lymphocytes at 1- 5 mM NP concentrations (e.g., $p = 0.003$ at 1 mM, $p = 0.0002$ at 2.5 mM, $p = 0.002$ at 5 mM, and $p = 0.05$; NK cells vs. CD3⁺ T cells at 10 mM NP). Most striking is the increased NP-induced cytotoxicity observed in monocytes, with >50% of the monocytes killed at the lowest NP concentration tested (0.5 mM). Statistically significant differences were observed between monocytes and NK cells (0.5 mM and 1 mM; $p = 0.0002$ and $p = 0.0008$, respectively), and monocytes compared to T and B lymphocytes ($p < 0.0001$ for both cell types at both concentrations tested).

Because adherent monocytes appear considerably more susceptible to NP-induced cytotoxicity compared to other immune cell subsets, additional experiments were performed using purified monocytes and lower concentrations of NP, to more accurately determine the IC₅₀ value. In these experiments, monocytes were treated with varying concentrations of ZnO NPs, and viability was evaluated using the fluorogenic redox Alamar Blue cytotoxicity assay. In agreement with monocyte data obtained from PBMC cultures, an IC₅₀ of ~0.30 mM was observed (Figure 3B). The Alamar Blue cytotoxicity assay was also used to confirm the IC₅₀ using purified CD4⁺ T cells, and a similar IC₅₀ value of ~5.4 was observed (data not shown). As previously reported by our lab [13,14,23], control experiments using bulk micron-sized ZnO powder showed no appreciable toxicity effect at any of the concentrations tested (e.g., viability with bulk ZnO: $96 \pm 3\%$ at 1 mM, $93 \pm 3\%$ at 10 mM), demonstrating that toxicity is limited to nanoscale ZnO. In addition, no appreciable toxicity was observed using NP-free supernatants (e.g., 98% viability with NP-free supernatant equivalent to 1-10 mM), indicating that the toxicity is likely not due to dissolved Zn ions from NP preparations.

Although these results indicate that monocytes are considerably more susceptible to NP-induced cytotoxicity than other immune cell types tested, it is important to note that these differences may be related to distinctions in cell-culture conditions. While T cells, B cells and NK cells grow as suspension cultures, cultured monocytes grow as an adherent monolayer. These differences in growth characteristics may act to increase the effective ZnO NP concentration in adherent cultures. It is also plausible that the inherently greater capacity of adherent monocytes to phagocytose foreign materials, including NPs, may underlie their greater sensitivity, and the inherent cytolytic activity of NK cells against foreign pathogens and altered self-cells may contribute to their greater sensitivity compared to lymphocyte populations. To address these possibilities, future experiments involving 3-dimensional cell culture systems and those evaluating the extent to which phagocytic/endocytic mechanisms contribute to cell-type differences are needed. Nevertheless, given the variable susceptibilities of different immune cell types to ZnO NPs, it

seems clear that careful analysis of *in vitro* cellular systems, followed by appropriate *in vivo* studies, is necessary to provide thorough and possibly predictive screening data regarding the relative toxicity and immunomodulatory effects of ZnO NP.

Memory and Naïve T cells Differ in Cytotoxic Response to ZnO NP

Our previous findings that ZnO NP toxicity is dependent on the cell activation status, with quiescent T cells being more resistant to ZnO NP-induced cytotoxicity than identical cells activated to divide via stimulation through the T cell receptor [13], led us to evaluate whether “memory” T cells display greater sensitivity to ZnO NPs than “naïve” T cells. During an immune response, the activation of T cells to a specific antigen found on a pathogen results in a cascade of intracellular signaling events, and to the differentiation of naïve T cells into memory cells. Once memory cells have formed, they can become activated to proliferate much more readily upon subsequent exposure to the original antigen [24]. This occurs because memory T cells require lower activation signals/thresholds to proliferate which is due, at least in part, to alterations in intracellular calcium mobilization and calcium-dependent signaling processes [25,26].

To assess potential susceptibilities of naïve and memory T cell populations to ZnO NPs in a well-controlled environment, PBMC (which contained both naïve and memory T cells) were treated with 8-nm ZnO NPs for 22-24 h, with the viability assessed by PI uptake using flow cytometry. Naïve CD3⁺ T cells (CD45RA⁺,CD3⁺) were identified based on the expression of the CD45RA surface marker, while memory T cells (CD45RO⁺,CD3⁺) were identified based on expression of the distinguishing CD45RO surface marker [26,27]. Cytotoxic responses were then compared to bulk cultures of CD3⁺ T cells containing both naïve and memory cells from the same blood donor. As shown in Figure 4, memory T cells displayed significantly greater sensitivity to NP toxicity than either naïve T cells or bulk cultures of CD3⁺ T cells ($p = 0.0044$ and $p = 0.0244$) at 10 mM ZnO NP concentration. Naïve T cells appeared more resistant than CD3⁺ T cells, although statistically significant differences were not observed ($p = 0.08$). These results demonstrate that even subsets of T cells show measureable differences in cytotoxic response to ZnO NP, which appears related to their activation threshold and/or proliferation potential.

ZnO NP Induce ROS Production in Monocytes and T Cells

Reactive oxygen species (ROS) are produced by cells as part of normal metabolic processes. However, in situations where ROS production exceeds the cell’s antioxidant capability, cell death can occur by interfering with normal physiological processes and the modification of cellular biomolecules [28]. Recently, several types of nanomaterials including quantum dots and metal-oxide NPs have been shown to induce intracellular generation of ROS [13,15,16,29], although only limited studies have evaluated the ability of ZnO NPs to induce ROS in normal/non-transformed human cells. To investigate oxidative stress as a mechanism of ZnO NP-induced cellular toxicity in normal immune cell populations, studies compared ROS production between primary monocytes and T cells. Based on the differing sensitivities of these two cell populations, two different concentrations of ZnO NPs were used (i.e., 1 mM and 5 mM). ROS generation was evaluated using the cell permeability dye, DCFH-DA, which is oxidatively modified into a highly fluorescent derivative by ROS including superoxide anion and hydrogen peroxide. Studies were performed using mixed PBMC cultures to allow for identical NP-treatment conditions, and cell identification was determined by staining with fluorescently labeled antibodies directed towards the CD3 and CD14 surface markers. Flow cytometry was then used to simultaneously identify monocytes and T cells, as well as their corresponding level of ROS production at both early and extended exposure times. As shown in Table 1, there was a modest amount of ROS produced in monocytes treated with 1 mM NP (19% ROS producing cells) as early as 6h post ZnO NP exposure, yet no detectable ROS was observed in T cells at the corresponding NP concentration and time point. However, at 20h of treatment, appreciable ROS production was observable in T cells (~38% ROS producing cells at 5 mM ZnO NP), yet no residual cell-associated ROS signal was observed in monocytes as nearly complete cell death was noted. These results indicate that ZnO NPs are capable of inducing intracellular ROS in both cell types, although ROS production in monocytes occurs considerably earlier than for T cells, which may mechanistically underlie their greater sensitivity to ZnO NPs.

ROS Quenchers Rescue Primary Monocytes and T Cells from ZnO NP Induced Cytotoxicity

Experiments were then performed to determine the causal role of NP-induced ROS as a major mechanism of toxicity. Purified human CD14⁺ monocytes and CD4⁺ T cells were pre-treated with N-acetyl cysteine (NAC), a well-known ROS quenching agent [30], prior to ZnO NP exposure. Following 24h of ZnO NP treatment, cell viability was assessed using the Alamar Blue cytotoxicity assay. Figure 5 reveals that 5 mM NAC significantly protects both monocytes and CD4⁺ T cells against cell death ($p = 0.0001$ and $p = 0.0481$, respectively), and implicates ROS formation as a major mechanism of ZnO NP-induced toxicity in primary immune cells.

ZnO NP Preferentially Associate with Monocytes Compared to Lymphocytes

Experiments were performed to gain insights into the mechanisms underlying the greater susceptibility of monocytes to NP-induced cytotoxicity, by evaluating the extent to which NPs preferentially associate with these cells. FITC-encapsulated ZnO NPs (FITC-ZnO NPs) were prepared as previously described by our group [23], and their fluorescence properties were used to monitor the extent to which they physically and stably associate with cells. Freshly isolated PBMC were treated with 5 mM FITC-ZnO NP, or left untreated, and multi-color flow cytometry was used to simultaneously identify monocytes and lymphocyte populations present in the PBMC culture, as well as the relative increase in the FITC-NP signal. As shown in Table 2, all immune-cell types evaluated showed a strong association with NPs, with 78-98% of cells displaying at least some level of positive FITC fluorescence compared to control cells cultured in the absence of NPs. However, a 9.3-13.7 - fold increase in the number of NP associating with any given monocyte compared to individual T or B lymphocytes was observed, as indicated by changes in mean fluorescence intensity (MFI) values. These results demonstrate that ZnO NPs preferentially associate with monocytes (MFI: 131.2), compared to lymphocyte subpopulations (MFI: 9.84 for CD3⁺ T cells, MFI: 14.1 for CD4⁺ T cells and MFI: 9.61 for B cells). The greater NP association with monocytes may arise through either extracellular membrane-NP interactions or intracellular NP uptake, as we have previously reported the ability of these same FITC-encapsulated NPs to be intracellularly localized in the human Jurkat T cell line using confocal microscopy [23].

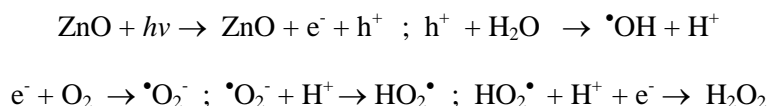
Effect of ZnO NP Size on Cytotoxicity and ROS Production

To evaluate the relationship between ZnO NP size and its toxic potential, three different sizes of ZnO NPs (4nm, 13nm, and 20nm) were concurrently evaluated using primary human CD4⁺ T cells as a model system. Experiments shown in Figure 6A were performed using a NP concentration of 5 mM, given the observed IC₅₀ value for T cells observed above. These experiments demonstrate that significantly greater cytotoxicity was observed with 4-nm NPs ($80.0\% \pm 2.0\%$), compared to either 13-nm or 20-nm sized NPs ($p=0.04$ and $p=0.01$, respectively). In addition, significantly more cytotoxicity ($p=0.05$) was observed for 13 nm NPs ($70.1\% \pm 8.0\%$), compared to 20-nm NPs ($44.0\% \pm 6.8\%$). To further verify that cytotoxicity increases with decreasing NP size, experiments were performed over a range of NP concentrations. As shown in Figure 6B, significantly greater toxicity was observed using 4-nm NPs compared to 20-nm NP at all concentrations tested ($p = 0.03$ at 1 mM, $p = 0.0001$ at 5 mM and $p = 0.01$ at 10 mM NP concentration). In this paper, we have focused on the size-dependence cytotoxicity of NPs. However, as shown in the inset to Figure 2, the aspect ratio of NPs increases with size. Therefore, the role of shape morphology on NP cytotoxic response will be the subject of future investigations.

To further evaluate the mechanism of nanotoxicity, studies were performed to investigate the relationship between size dependence and ZnO NP-induced ROS production using PBMC cell cultures. Following a 3h treatment with different-sized ZnO NPs (4-nm, 13-nm and 20-nm), a size-dependent induction of ROS was observed at both NP concentrations, with 4-nm sized NPs consistently inducing higher levels of ROS compared to 13-nm or 20-nm sized NPs (Figure 7). At 5 mM NP concentrations, significantly higher levels of ROS were observed for 4-nm and 13-nm NPs compared to 20-nm NPs (~4-fold relative increase ($p = 0.005$) and ~3-fold increase ($p = 0.01$), respectively). Similarly, 10 mM NP treatment resulted in significant differences in ROS production between all sizes of NP with a 3.2-fold greater induction of ROS observed between 4-nm and 20-nm NPs ($p = 0.001$), and a 1.9-fold increase observed between 13-nm and 20-nm NPs ($p = 0.0021$). This findings indicate that the generation of ROS is dependent on NP size.

The increased nanotoxicity with decreasing NP size may be due in part to, the larger surface area/volume ratio of smaller NPs which provides them with a greater area to associate with cellular membranes and proteins, as well as greater surface reactivity. In addition, ZnO particles prepared in a nonaqueous medium may have oxygen deficient/zinc rich surface chemistries [10] that exhibit strong electrostatic interactions with the negatively charged cell membrane [31,32], with smaller particles predicted to have a greater positive surface charge to volume ratio. Thus, greater initial cell membrane-NP association would be expected for smaller NP, leading to potentially greater intracellular uptake.

Following initial NP-cell electrostatic interactions, mechanisms of toxicity likely proceed via the formation of highly reactive oxygen species, such as hydrogen peroxide, hydroxyl radical, and superoxide anion [2,16]. The ability of smaller-sized ZnO NPs to promote greater levels of ROS may occur because as ZnO NP size decreases, so does the nanocrystal quality, which results in increased interstitial zinc ions and oxygen vacancies [33]. These crystal defects lead to a large number of electron-hole pairs (e^- - h^+) which are typically activated by both UV and visible light. However, for nanoscale ZnO, large numbers of valence band holes and/or conduction band electrons are thought to be available to serve in redox reactions even in the absence of UV irradiation [17]. The holes can split water molecules derived from the ZnO suspension into H^+ and OH^- . The resulting electrons react with dissolved oxygen molecules to generate superoxide radical anions ($\bullet O_2^-$), which in turn react with H^+ to generate ($HO_2\bullet$) radicals. These $HO_2\bullet$ molecules can then produce hydrogen peroxide anions (HO_2^-) following a subsequent encounter with electrons. Hydrogen peroxide anions can then react with hydrogen ions to produce hydrogen peroxide (H_2O_2) [7,34].



All of the various ROS molecules produced in this fashion can trigger redox-cycling cascades in the cell, or on adjacent cell membranes. This can then lead to the depletion of endogenous cellular reserves of antioxidants such that irreparable oxidative damage occurs to cellular biomolecules and eventually results in cell death.

ZnO NP Induce Pro-Inflammatory Cytokine Production in Primary Human Immune Cells

An important task of nanobiotechnology is to understand the effect these nanomaterials have to modulate expression of cytokines, which are soluble biological protein messengers that regulate the immune system. Published studies have demonstrated the ability of certain nanomaterials to induce cytokine production, although this appears heavily dependent on a variety of factors, including material composition, size, and method of delivery [35,36]. Much remains to be learned, however, regarding the pro-inflammatory potential of ZnO NPs. To address this gap in knowledge, studies were performed to evaluate the ability of ZnO NPs to modulate IFN- γ , TNF- α and IL-12 cytokine production in primary human immune cells. These particular cytokines were chosen because they represent critical pathways involved in the inflammatory response and differentiation processes. Freshly isolated PBMC were treated with varying concentrations of 8-nm ZnO NPs for 38h, and cell-free supernatants were used to quantitate cytokine levels using an ELISA. For IL-12 production, cell samples were first pre-treated with IFN- γ (1000 U/mL) before addition of NPs to provide a priming signal for IL-12 [37]. Results demonstrate significant dose-dependent increases in IFN- γ and TNF- α at all NP concentrations tested (0.05 mM, 0.1 mM and 0.2 mM) (Figure 8). ZnO NPs had no effect on IL-12 production in unprimed control cultures, but pretreatment with low level IFN- γ prior to NP exposure resulted in appreciable amounts of IL-12 in a concentration-dependent manner. The inability of ZnO NPs to induce IL-12 in resting cells was not altogether unexpected, as expression of this cytokine typically occurs in cells that have first received a priming signal, such as IFN- γ , which is locally produced by other cells participating in the immune response [37]. These results suggest that a synergistic relationship between ZnO NPs and IFN- γ may occur in *in vivo* settings employing ZnO NPs, and demonstrate that ZnO NPs are capable of inducing at least some key components of inflammation.

The ability of ZnO NPs to induce proinflammatory cytokine expression in human primary immune cells is consistent with the recognized relationship between oxidative stress and inflammation, which is partially mediated by induction of the NF- κ B transcription factor [38]. To date, only limited studies have evaluated the effects of ZnO NPs on cytokine production, and most of these studies have been conducted in non-hematological cell types or in immortalized cell lines which frequently display alterations in signal transduction pathways, leading to unpredictable changes in protein expression. In one report, ZnO NPs were shown to increase IL-8 and MCP-1 cytokine mRNA expression in human aortic endothelial cells, although no information was provided regarding changes in corresponding protein levels [39]. In two other studies conducted in immortalized rodent lung epithelial cells, alveolar macrophage cell lines and primary alveolar macrophages, ZnO NPs fail to induce TNF- α at concentrations exceeding those used in this study [36,40]. In addition, no changes in other cytokines and chemokines including IL-6, G-CSF, MIP-2, CXCL10, and CCL2 were detected. The ability of ZnO NPs to induce high levels of TNF- α in our studies may be due to differing responses observed between cell populations studied (i.e., PBMC vs. alveolar macrophages), or reflect the longer NP treatment exposure period (i.e., 38h vs. 24h). Although, to the best of our knowledge, no published studies have demonstrated the ability of ZnO NPs to induce TNF- α or IL-6 production in purified primary cell cultures or in toxicological evaluations, it is interesting to note that inhalation of ultrafine ZnO particles in occupational settings can increase the expression of these cytokines, which is symptomatically recognized as metal fume fever in welders (e.g., fatigue, fever, chills, myalgias, cough, and leukocytosis) [16].

The ability of ZnO NPs to induce IL-12, IFN- γ , and TNF- α at NP concentrations below those causing appreciable cytotoxicity indicates immunomodulatory effects that may function to bias the immune response towards Th1-mediated immunity. It is the cytokine profile that directs the development and differentiation of T helper cells into the two different subsets, called type 1 (Th1) and type 2 (Th2) [41,42]. Th1 cells are recognized to play an essential role in promoting innate and cell-mediated immunity, while Th2 cells promote antibody-based humoral responses [41]. Relevant to our findings, IL-12 and IFN- γ play critical roles in Th1 development, and help set-up a perpetuating loop whereby more Th1 development is favored, Th2 development is suppressed, and the cytotoxicity activity of both NK cells and T cytotoxic cells against cancerous cells, virally infected cells, or intracellular pathogens is enhanced [42]. Thus, our findings indicate that careful titration of ZnO NP-based therapeutic interventions may be successful in elevating a group of cytokines important for eliciting a Th1-mediated immune response with effective anti-cancer actions. These results, combined with our previous observations demonstrating that immortalized hematopoietic cancer cells are preferentially killed (~33-fold) by ZnO NPs compared to normal cells of identical lineage [13], suggest that ZnO NPs may function via a two-fold mechanism to eliminate cancer cells by direct and preferential cytotoxic actions, and by enhancing the type of immunity most effective at eliciting an *in vivo* anti-cancer response.

The ability of ZnO NPs to induce TNF- α may also help promote Th1 differentiation [41,43] as well as functioning as a regulator of acute inflammation [44]. Notably, this cytokine received its name based on its potent *in vitro* and *in vivo* anti-tumor activity. However, high level and/or chronic exposure to TNF- α has been shown to produce serious detrimental effects on the host, including septic shock or symptoms associated with autoimmune disease [44]. Our results demonstrate significant dose-dependent increases in TNF- α over a somewhat narrow range of ZnO NP concentrations. The magnitude of TNF- α induction, as well as other pro-inflammatory cytokines, and their local-regional delivery to tumor sites or other desired areas, will undoubtedly be important parameters when considering ZnO NP for biomedical purposes to achieve the desired therapeutic response without eliciting potential systemic damaging effects from these cytokines.

Conclusions

Results from these studies demonstrate that ZnO NPs induce toxicity in a cell-type specific manner that is dependent on the degree of NP-cellular membrane association, phagocytic ability, and inherent cellular capacities for ROS production. Monocytic cells displayed the greatest susceptibility and intracellular ROS production following NP exposure, followed by NK cells, followed by lymphocytes, which displayed the most resistance. Studies employing ROS quenchers implicate ROS formation as a major mechanism of

ZnO NP-induced toxicity, and demonstrate that the generation of ROS and the cytotoxic profile occurs in a NP size-dependent manner, with smaller NPs displaying the greatest effect. The variable responses of immune cells described in this study underscore the need for careful *in vitro* evaluation across a spectrum of relevant cell types, followed by appropriate *in vivo* studies to provide useful and potentially predictive screening data regarding the relative toxicity effects of metal-oxide NPs. These factors are also important considerations for the potential incorporation of ZnO NPs into novel nanotechnology-based biological applications.

Our results demonstrating that ZnO NPs can induce the expression of immunoregulatory cytokines is also a relevant consideration for potential use in biomedical applications, as many current treatments for human disease function by manipulating and controlling components of the immune response [45]. To the best of our knowledge, our results appear to be the first to document the ability of ZnO NPs to increase the expression of IFN- γ , TNF- α , and IL-12 in primary immune human cells, and at NP concentrations below those causing appreciable cell death. These findings suggest that ZnO NPs, when used at appropriate concentrations, could directly enhance tumor cell killing through the production of TNF- α , and could also facilitate effective anti-cancer actions by eliciting a cytokine profile crucial for directing the development of Th1-mediated immunity. The *in vivo* therapeutic window for ZnO NP to increase proinflammatory cytokines indicates that parameters controlling ZnO NP toxicity, such as particle size, concentration, and biodistribution will need to be carefully controlled when considering metal-oxide NPs for use in biological applications, especially given the recognized relationship of chronic inflammatory processes and tumorigenesis. Future studies are needed to investigate the effects of ZnO NPs on additional cytokines and inflammatory mediators, as well as mechanisms of NP cellular uptake and ROS formation.

Figure Legends

Figure 1. TEM images of ZnO nanoparticle samples made using the hydrolysis molar ratio (water:zinc acetate) of 2.4 (panel a), 6.1 (panel b), 12.2 (panel c), and 24.4 (panel d). Panel (e) shows the corresponding size distribution of the samples shown in panel a (4 nm), panel b (8 nm), panel c (13 nm) and panel d (20 nm). Panel (e) shows a histogram obtained from TEM data demonstrating particle size distribution.

Figure 2. X-ray diffraction θ - 2θ scans of powder samples of various sizes of ZnO nanoparticles recorded in air at room temperature. The x-ray source used was Cu K α with an effective wavelength $\lambda = 1.5418 \text{ \AA}$. The peak widths are inversely related to the crystallite sizes according to the Scherrer relation, enabling the XRD patterns to demonstrate the change in particle size. The stick pattern from reference data for wurtzite ZnO is shown along the x -axis (represented by the solid squares) and fully indexes the experimental data. The inset shows the relationship between average crystallite size (L) and average aspect ratio (AR) of several samples, prepared using the synthesis method employed in this work, as determined by XRD. AR was calculated from the widths of the (100) and (002) XRD peaks, and excludes data for 4 nm samples due to the amount of peak overlap.

Figure 3. Differential cytotoxic effects of ZnO NPs on human immune cell subsets. **A)** PBMC were treated with varying concentrations of 8-nm ZnO NPs for 24h and viability of CD3⁺ T cells, CD4⁺ T cells, B cells, NK cells, and monocytes present in same PBMC cultures determined by monitoring PI uptake using flow cytometry. Data from three independent experiments is presented with error bars depicting standard error (s.e.). Asterisks denote statistically significant ($p < 0.05$) differences between CD3⁺ T cells, B cells, NK cells and monocytes at indicated NP concentrations as determined using a repeated measures ANOVA. **B)** ZnO NP toxicity on purified human primary monocytes. Purified human peripheral blood CD14⁺ monocytes were treated with varying concentrations of ZnO NPs (0.0625 -1 mM) and viability assessed using the Alamar Blue cytotoxicity assay with error bars representing s.e., ($n=4$). The IC₅₀ was determined using non-linear regression analysis.

Figure 4. Differential ZnO NP cytotoxicity between naïve and memory T cells. Human peripheral blood PBMC were left untreated or treated with 10 mM ZnO NPs (8-nm) for 22-24h and viability determined by monitoring PI uptake using flow cytometry. T cells were defined as CD3⁺, naïve T cells as

CD3⁺,CD45RA⁺, and memory T cells as CD3⁺,CD45RO⁺. Data from three independent experiments is presented and error bars depict s.e. Asterisks denote statistically significant differences (p<0.05) between NP treatment groups using as a one-way repeated measures ANOVA.

Figure 5. Quenching of ROS rescues T cells and monocytes from ZnO NP-induced cytotoxicity. Purified peripheral blood CD14⁺ monocytes (≥ 96% purity) and CD4⁺ T cells (≥ 95% purity) were pretreated for 4-6 hr with 5 mM N-acetyl cysteine (NAC) or vehicle control and then subsequently cultured with 8-nm sized ZnO NPs, or left untreated for 24 hr. Viability was assessed using the Alamar Blue cytotoxicity assay. **A)** Purified monocytes treated with 0.125 mM ZnO NPs ± 5 mM NAC, n=3. **B)** Isolated CD4⁺ T cells treated with 5 mM ZnO NPs ± 5 mM NAC, n=3. Asterisks denote statistically significant differences (p<0.05) as analyzed using a 2-way ANOVA and error bars depict s.e.

Figure 6. Effect of NP size on cytotoxicity. **A)** Purified human CD4⁺ T cells (>97% purity) were left untreated or incubated with different sizes (4, 13, and 20 nm) of ZnO NPs at a final concentration of 5 mM. Following culture for 22-24 hr, viability was determined using PI uptake and flow cytometry, n=4. **B)** Cytotoxicity studies in purified human CD4⁺ T cells were performed using varying concentrations (1-10 mM) of 4-nm and 20-nm sized ZnO NPs, n=4. Error bars depict s.e. and asterisks indicate statistically significant differences (p<0.05) as determined by repeated measures ANOVA.

Figure 7. Effects of NP size on ROS production in peripheral blood immune cells. Primary human PBMC were treated with two different concentrations of ZnO NPs (5 mM and 10 mM) for 3h and ROS production evaluated using a fluorescent microplate reader. Data from a representative experiment is shown (n = 3) with error bars depicting s.e. Data was analyzed using a 2-way ANOVA and asterisks denote statistical significance as defined by p<0.05.

Figure 8. ZnO NPs increase pro-inflammatory cytokine production in primary human peripheral blood cells. PBMC were left untreated or treated with varying concentrations of 8-nm ZnO NPs, both alone or with the addition of exogenous IFN-γ (1000 U/mL), for 38h. Cytokine production was evaluated by ELISA and data analyzed using a 2-way ANOVA. Error bars depicting s.e., n=3. Asterisks denote statistically significant differences as defined as p<0.05.

Table 1. Freshly isolated PBMC were treated with 1mM and 5 mM of 8-nm sized ZnO NPs and ROS production measured using the oxidation sensitive DCFH-DA probe. Following NP treatment for 6h or 20h, cells were loaded with DCFH-DA and flow cytometry used to simultaneously evaluate ROS production and distinguish T cells and monocytes present in PBMC cultures by staining with fluorescently labeled CD3 and CD14 antibodies. Values indicate the percentage of ROS producing cells ± s.e., n=3.

Table 2. Freshly isolated PBMC were left untreated or exposed to 5 mM FITC-encapsulated ZnO NPs for 15h. The cell mixture was then stained with fluorescently labeled CD3, CD4, CD19, CD14 antibodies to identify subsets, washed to remove excess antibody and unbound NPs, and the level of NP association determined based on FITC fluorescent signal using flow cytometry. Data was obtained by gating on 10,000 events, n=3.

Acknowledgements

This research was supported in part by the Mountain States Tumor and Medical Research Institute, Boise, ID, NSF grants (DMR-0605652 and MRI 0821233) and NIH (1R15 AI06277-01A1).

Reference

1. S. E. McNeil. J. Leukoc. Biol. 78, 585 (2005)
2. T.K. Jain, M.A. Morales, S.K. Sahoo, D.L. Leslie-Pelecky, V. Labhasetwar. Mol. Pharm. 2, 194 (2005)

3. J.B. Baxter, E.S. Aydil. *Appl.Phys.Lett.* 86, 53114. (2005)
4. W.T. Liu. *J. Biosci. Bioeng.* 102, 1(2006)
5. G.J. Nohynek, E.K. Dufour, M.S. Roberts. *Skin Pharmacol. Physiol.* 21, 136 (2008)
6. G.J. Nohynek, J. Lademann, C. Ribaud, M.S. Roberts. *Crit. Rev. Toxicol.* 37, 251 (2007)
7. N. Padmavathy, R. Vijayaraghavan. *Sci. Technol. Adv. Mater* 9, 1 (2008)
8. V. Wagner, A. Dullaart, A.K. Bock, A. Zweck. *Nat. Biotechnol.* 24, 1211 (2006)
9. D. Peer, J.M. Karp, S. Hong, O.C. Farokhzad, R. Margalit, R. Langer. *Nat. Nanotechnol.* 2, 751 (2007)
10. S. Nair, A. Sasidharan, R. Divya, V.D. Menon, S. Nair, K. Manzoor, S. Raina. *J. Mater. Sci. Mater. Med.* 10,10856 (2008)
11. A. Nel, T. Xia, L. Madler, N. Li. *Science* 311, 622 (2006)
12. E. Oberdorster. *Environ. Health Perspect.* 112, 1058 (2004)
13. C. Hanley, J. Layne, A. Punnoose, K.M. Reddy, I. Coombs, A. Coombs, K. Feris, D. Wingett. *Nanotechnology* 19, 295103 (2008)
14. K.M. Reddy, K. Feris, J. Bell, D.G. Wingett, C. Hanley, A. Punnoose. *Applied Physics Letters* 90, 213902 (2007)
15. T.C. Long, N. Saleh, R.D. Tilton, G.V. Lowry, B. Veronesi. *Environ. Sci. Technol.* 40, 4346 (2006)
16. T. Xia, M. Kovochich, J. Brant, M. Hotze, J. Sempf, T. Oberley, C. Sioutas, J.I. Yeh, M. . Wiesner, A.E. Nel. *Nano. Lett.* 6, 1794 (2006)
17. H. Yang, C. Liu, D. Yang, H. Zhang, X Zhuge. *J. Applied Toxicol.* 29, 69 (2008)
18. J. Jiang, G. Oberdorster, P. Biswas. *J. Nanopart. Res.* 11, 77 (2009)
19. J.E. Coligan, *Current Protocols in Immunology*, Greene Publishing Associates and Wiley-Interscience, New York (1995)
20. J. Luo, N. Li, R.J. Paul, R. Shi. *J. Neurosci. Methods* 120, 105 (2002)
21. H. Hong, G.Q. Liu. *Life Sci.* 74, 2959 (2004)
22. I. Onaran, S. Sencan, H. Demirtas, B. Aydemir, T. Ulutin, M. Okutan. , *Naunyn Schmiedebergs Arch. Pharmacol.* 378, 471 (2008)
23. H. Wang, D. Wingett, M.H. Engelhard, K. Feris, K. . Reddy, P. Turner, J. Layne, C. Hanley, J. Bell, D. Tenne, C. Wang, A. Punnoose. *J. Mater. Sci: Mater. Med.* 20, 11 (2009)
24. C.D. Surh. *J. Sprent. Immunity.* 29, 848 (2008)
25. S.R. Hall, B.M. Heffernan, N.T. Thompson, W.C. Rowan. *Eur. J. Immunol.* 29, 2098 (1999)
26. A. Sigova, E. Dedkova, V. Zinchenko, I. Litvinov. *FEBS Lett.* 447, 34 (1999)
27. D.D. Cataldo, J. Bettiol, A. Noel, P. Bartsch, J.M. Foidart, R. Louis. *Chest* 122, 1553 (2002)

28. S.W. Ryter, H.P. Kim, A. Hoetzel, J.W. Park, K. Nakahira, X. Wang, A.M. Choi. *Antioxid. Redox. Signal.* 9, 49 (2007)
29. J. Lovric, S.J. Cho, F.M. Winnik, D. Maysinger. *Chem. Biol.* 12, 1227 (2005)
30. M. Valko, D. Leibfritz, J. Moncol, M. . Cronin, M. Mazur, J. Telser. *Int. J Biochem. Cell Biol.* 39, 44 (2007)
31. N. Papo, M. Shahar, L. Eisenbach, Y. Shai. *J. Biol. Chem.* 278, 21018 (2003)
32. J.O.M. Bockris, M.A. Habib. 10, 227 (1982)
33. S.K. Sharma, P.K. Pujari, K. Sudarshan, D. Dutta, M. Mahapatra, S.V.Godbole. *Solid State Communications* 149, 550 (2009)
34. I.A. Salem. *Monatshefte fur Chemie* 131, 1139 (2000)
35. R. Duffin, L. Tran, D. Brown, V. Stone, K. Donaldson. *Inhal. Toxicol.* 19, 849 (2007)
36. C.M. Sayes, K.L. Reed, D.B. Warheit. *Toxicol. Sci.* 97, 163 (2007)
37. E. Maranda, T. Robak. *Postepy Hig. Med. Dosw.* 52, 489 (1998)
38. A. Federico, F. Morgillo, C. Tuccillo, F. Ciardiello, C. Loguercio. *Int. J Cancer* 121, 2381 (2007)
39. A. Gojova, B. Guo, R.S. Kota, J.C. Rutledge, I.M. Kennedy, A.I. Barakat. *Environ. Health Perspect.* 115, 403 (2007)
40. A.Beyerle, H. Schulz, T. Kissel, T. Stoeger. *Inhaled Particles* 151, 1 (2009)
41. M.B. Lappin J.D. Campbell. *Blood Rev.* 14, 228 (2000)
42. M.A. Fishman, A.S. Perelson. *Bull. Math. Biol.* 61, 403 (1999)
43. C. Dong, R.A. Flavell. *Curr. Opin. Hematol.* 8, 47 (2001)
44. M. Croft. *Nat. Rev. Immunol.* 9, 271 (2009)
45. Y. Becker. *Anticancer Res.* 26, 1113 (2006)